7-25-2016

Blinking Phase-Change Nanocapsules Enable Background-Free Ultrasound Imaging

Alexander S. Hannah
Georgia Institute of Technology

Geoffrey P. Luke
Dartmouth College

Stanislav Y. Emelianov
Georgia Institute of Technology

IVYSPRING INTERNATIONAL PUBLISHER

Theranostics

2016; 6(11): 1866-1876. doi: 10.7150/thno.14961

Research Paper

Blinking Phase-Change Nanocapsules Enable Background-Free Ultrasound Imaging

Alexander S. Hannah[1,2,4], Geoffrey P. Luke[3,4], Stanislav Y. Emelianov[1,2,4]✉

1. School of Electrical and Computer Engineering, Georgia Institute of Technology, Atlanta, GA, 30332.
2. Wallace H. Coulter Department of Biomedical Engineering, Georgia Institute of Technology and Emory University School of Medicine, Atlanta, GA 30332.
3. Thayer School of Engineering, Dartmouth College, Hanover, NH, 03755.
4. Department of Biomedical Engineering, The University of Texas at Austin, Austin, TX, 78712.

✉ Corresponding author: stas@gatech.edu.

Received: 2016.01.13; Accepted: 2016.05.12; Published: 2016.07.25

Abstract

Microbubbles are widely used as contrast agents to improve the diagnostic capability of conventional, highly speckled, low-contrast ultrasound imaging. However, while microbubbles can be used for molecular imaging, these agents are limited to the vascular space due to their large size (> 1 μm). Smaller microbubbles are desired but their ultrasound visualization is limited due to lower echogenicity or higher resonant frequencies. Here we present nanometer scale, phase changing, blinking nanocapsules (BLInCs), which can be repeatedly optically triggered to provide transient contrast and enable background-free ultrasound imaging. In response to irradiation by near-infrared laser pulses, the BLInCs undergo cycles of rapid vaporization followed by recondensation into their native liquid state at body temperature. High frame rate ultrasound imaging measures the dynamic echogenicity changes associated with these controllable, periodic phase transitions. Using a newly developed image processing algorithm, the blinking particles are distinguished from tissue, providing a background-free image of the BLInCs while the underlying B-mode ultrasound image is used as an anatomical reference of the tissue. We demonstrate the function of BLInCs and the associated imaging technique in a tissue-mimicking phantom and *in vivo* for the identification of the sentinel lymph node. Our studies indicate that BLInCs may become a powerful tool to identify biological targets using a conventional ultrasound imaging system.

Key words: Microbubbles, ultrasound imaging

Introduction

Ultrasound contrast agents provide acoustic backscatter due to a mismatch in impedance between the gas core of microbubbles and the surrounding, water-based soft tissue. Contrast is also enhanced due to compressibility of their gaseous cores compared to surrounding tissues, resulting in mechanical oscillations of the bubbles. Signal enhancement from microbubbles was first demonstrated using echocardiography in 1968.(1) Since then, a variety of microbubbles and molecular targeting strategies have been explored to assist in the identification of early disease states.(2) However, despite the echogenicity of microbubbles against a soft tissue background, the local image contrast is hindered by the abundant sub-wavelength acoustic scatterers in most biological tissues.(3–5) To combat this issue, several functional contrast agents and nonlinear imaging techniques have been implemented. For example, harmonic and pulse inversion imaging utilize the nonlinear oscillatory behavior of microbubbles in response to ultrasound irradiation, which can help distinguish them from the background tissue.(6,7) However, the harmonic response of tissues limits the specificity of this technique, and tissue motion degrades the detection of microbubbles.(8–10) Additionally, microbubbles are confined to the vascular space due

to their large size,(11) and their circulation time is limited to a few minutes as gas diffuses from the bubble core.(12)

A new generation of nano-sized triggerable particles, referred to as phase-change nanodroplets, is emerging to address these limitations. These stable liquid droplets vaporize in response to either a pulsed laser or ultrasound, providing contrast enhancement activated by an external trigger.(13–17) When droplets are vaporized using a pulsed laser, they simultaneously emit a strong photoacoustic signal, facilitating multimodal imaging.(13,14,18) Their small size enables access to extravascular targets, and their liquid core results in a more stable particle (hours) (Supplementary Information, Fig. S1) than conventional microbubbles.(12) Several groups have previously developed perfluorocarbon (PFC) droplet nanoemulsions for imaging and therapeutic applications. Work by Sheeran et al. reports well characterized, acoustically activatable PFC emulsions for ultrasound and pulse inversion imaging applications.(19) Rapoport et al. have encapsulated therapeutics for a highly stable particle capable of simultaneous imaging and ultrasound-triggered drug delivery.(20) Other groups have encapsulated photoabsorbers for optical activation. Wilson et al. first reported laser-induced droplet vaporization for simultaneous ultrasound and photoacoustic imaging.(14) Strohm et al. reported similar results using droplets with incorporated quantum dots activated by 1064 nm light for improved photoacoustic contrast.(15) Akers et al. used a high boiling point PFC with encapsulated dye for a stable particle capable of extended photoacoustic contrast.(21) Larson-Smith et al. report the well-studied synthesis of a gold-nanoparticle stabilized nanoemulsion.(22) To enable extended imaging, several groups have used higher boiling point PFC particles capable of repeated vaporization. Rapoport et al. demonstrated repeated ultrasonic activation of a highly stable particle.(20) Asami et al. incorporated a dye into a high boiling point PFC droplet and vaporized it repeatedly for prolonged photoacoustic contrast.(23) Arnal et al. report the synthesis of a gold particle shelled PFC emulsion and a high contrast, real-time ultrasound/photoacoustic imaging technique using synchronized laser pulses.(24,25) Each of these strategies utilizes a combination of particle properties, laser energy, optical triggering, and ultrasound imaging techniques to obtain high contrast biomedical image information. This work aims to improve image contrast, depth sensitivity, and particle stability to enhance diagnostic information.

Here we report stable, dynamic contrast agents called BLInCs, which respond to optical irradiation for a background-free, ultrasound-based image of the particles. The BLInCs consist of a liquid perfluorohexane (PFH) core, which has a bulk boiling point of 56°C, resulting in a stable liquid droplet at physiological temperatures (Fig. 1a). The submicron BLInCs are encapsulated by a fluorosurfactant polymer shell, which lowers the interfacial surface tension.(26) The high curvature of the interface increases the Laplace pressure between the PFH core and the surrounding water, further stabilizing the particles in a nano-sized state.(27) The BLInCs incorporate a near-infrared absorbing dye and can be activated by irradiating them with a pulsed laser. In response to irradiation (Fig. 1a), the dye catalyzes rapid (< 1-2 μs) droplet vaporization (Fig. 1b-c), behavior observed in other PFC particles.(13–15) The resulting transient gaseous microbubbles (Fig. 1c), which persist for up to several milliseconds, reflect ultrasound waves before recondensing back into their stable, weakly scattering nanodroplet form (Fig. 1d). This two-part phase change (liquid → gas → liquid) "blinking" process can be measured (Fig. 1e) using any clinical ultrasound imaging system capable of high speed imaging techniques, such as ultrafast or parallel beam imaging. The BLInCs can be activated repeatedly by a series of laser pulses, inducing brief moments of high echogenicity during their gaseous phase. When imaged, this behavior differentiates them from tissue, and the data can be processed to form a background-free image of the BLInCs. When combined with their size, the controllable dynamics of the BLInCs may enable a wide array of high contrast molecular ultrasound imaging and therapeutic applications.

Materials and Methods

Synthesis of BLInCs

First, 1 mg of Epolight 3072 dye (Epolin, Inc.) was added to 300 μL of PFH (FluoroMed, L.P.) and dissolved by sonication at 180 W for 30 s in a VWR benchtop ultrasonic cleaner. Then 1 mL of 1% v/v aqueous Zonyl FSO fluorosurfactant (Sigma) and 1.7 mL of deionized water were added to the PFH. The mixture was emulsified by vortexing for 10s and sonicated for 2 minutes at 180 W in a VWR benchtop ultrasonic cleaner. The nanodroplets were washed of excess dye and fluorosurfactant by centrifuging at 1000 rcf for 5 minutes and replacing the supernatant with deionized water. The BLInCs were diluted and then manually counted under a light microscope to obtain an estimate of their concentration after synthesis.

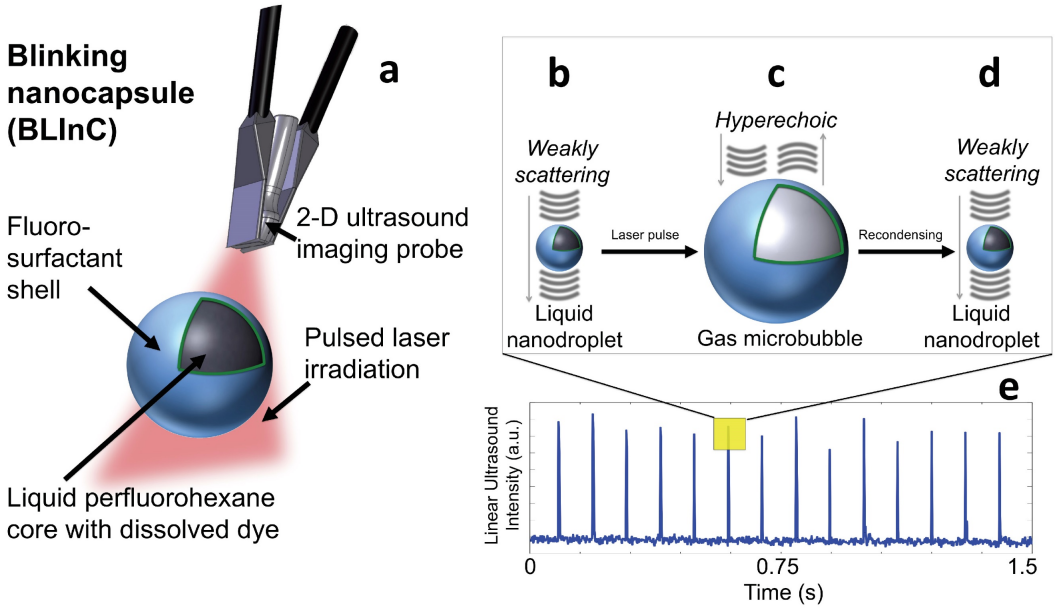

Figure 1. (a) The BLInCs comprise a liquid PFH core with an encapsulated near-infrared dye stabilized by a surfactant shell. The particles are activated using a pulsed laser. In their native state (b), the liquid BLInCs are weakly scattering and largely undetectable by ultrasound. Upon activation (c), the BLInCs undergo a rapid liquid-gas phase change, rendering them temporarily hyperechoic. The BLInCs recondense back to their native liquid state (d), able to be activated again. (e) Pulse-echo ultrasound image intensity from the periodic, laser-induced two-part phase changes.

Characterization of dye's optical absorption and BLInCs' size

A small amount of the dye was dissolved in chloroform and its extinction spectrum was measured with a UV-3600 UV-Vis spectrometer (Shimadzu). A Zetasizer Nano ZS system (Malvern Instruments Ltd.) was used to measure the diameters of a 1% v/v solution of as-prepared BLInCs, at 15 measurements per run. An intensity-weighted distribution is reported.

Optical verification of BLInC phase change behavior

A DMI 3000B inverted light microscope microscope (Leica Microsystems) was used to observe a 0.01% v/v solution of perfluoropentane droplets. A 50 mJ/cm^2 pulsed laser irradiated the sample to form stable bubbles, and another image was collected several minutes later. The temperature of the bubbles was reduced to induce bubble recondensation. Approximately 1 minute later, a final image of the liquid droplets was collected.

Synthesis of Phantoms Containing BLInCs

Two types of phantoms were constructed: one with a uniform distribution of BLInCs, and another consisting of a BLInC-labeled cylindrical inclusion within a BLInC-free background. To construct the phantoms, 64 mL of water was mixed with 21 mL of 40% acrylamide (Ambion) and 850 µL of 438 mM aqueous ammonium persulfate (Sigma-Aldrich). The solution was stirred in a Büchner flask with a rubber stopper to seal the top, and a tube connected to the side attached to a vacuum. The solution was sonicated under vacuum for 5 minutes to remove dissolved gas, and then the vacuum was removed to stir in additional components, using one of two formulations listed below.

Phantom with uniform incorporation of BLInCs: A solution of as-prepared, 180 nm diameter BLInCs was added to the solution so that the entire phantom contained 0.1% or 0.001% v/v of the as-prepared BLInCs solution. Next, 106 µL of tetramethylethylene-diamine (TEMED) (Sigma) was added. The entire solution was quickly poured into a rectangular mold and allowed to polymerize for 10 minutes.

Phantom containing BLInC-labeled cylindrical inclusion within BLInC-free background: 5 µm Min-U-Sil silica particles (U.S. Silica) were added at 0.2% w/w, and graphite particles (Dixon) were added at 0.01% w/w to mimic the optical absorption (2-3 cm^{-1}) and acoustic scattering (1-2 dB MHz^{-1}) of biological tissue.(28,29) Next, 106 µL of TEMED was added. The solution was quickly poured into a rectangular mold, where a 1.2 mm diameter sealed glass tube was positioned to create a cylindrical void in the phantom. After polymerizing, another solution was prepared which included 0.1% v/v of 180 nm diameter BLInCs and excluded graphite particles. The solution was poured into the cylindrical cavity, and allowed to polymerize. The final concentration of BLInCs in the inclusion was approximately 10^8/mL.

Imaging of BLInCs in Phantom

Each phantom was placed under a 40 MHz imaging probe connected to a Vevo 2100 ultrasound imaging system. The imaging probe and phantom surface were coupled using clear ultrasound gel. Optical fiber bundles were used to deliver 1064 nm pulsed laser light from a Phocus Mobile laser system (Opotek Inc.) to the phantom. Ultrasound B-mode data was collected while the phantom was irradiated with 5 ns laser pulses at a rate of 10 Hz. Image data from 1000 frames over a period of ~3.5 seconds were collected. For the phantoms with uniformly distributed BLInCs, the laser fluence was varied from 5 to 20 mJ/cm^2, with a frame rate of either 380 or 650 frames/second. The ultrasound window was 3.08 mm wide, 15 mm deep with a 1 mm offset, and a 10 mm focal depth. For the phantom with a cylindrical inclusion, the laser fluence was 50 mJ/cm^2, the frame rate was 580 frames/second, and the ultrasound window was 4.08 mm wide, 15 mm deep with a 1 mm offset, with a focal depth of 13 mm. For the phantom with the inclusion, the estimated fluence at the depth of the inclusion was 6-12 mJ cm^{-2}.

To visualize a three-dimensional volume, 21 image slices were collected 160 µm apart for a total elevational distance of 3.2 mm. At each location, a set of 1000 frames was acquired. The 2D or 3D IQ B-mode data was obtained for processing, and linear image intensity was calculated by $(I^2 + Q^2)^{1/2}$. The image data were further analyzed by custom-designed MATLAB functions and routines. Three-dimensional images were created using Amira (FEI Visualization Sciences Group).

Formation of Background-Free Ultrasound Image of BLInCs

To identify the location of the BLInCs in an otherwise low contrast ultrasound image, a set of B-mode ultrasound images was analyzed. This technique utilizes the transmission of multiple US waves, followed by subtraction of subsequent received signals, similar to that used in pulse inversion imaging.(6) Positive values of the differential intensity denote increases in echogenicity from vaporization, and negative spikes correspond to recondensation of the bubbles into droplets. Pixels not containing BLInCs, even though equally irradiated by the laser light, did not exhibit these changes. To form a map of the particles, two separate images were first constructed. The first image was formed by calculating a mean of the absolute value of the difference values at frames corresponding to activation by the laser. To make the second image, a temporal autocorrelation of the absolute value of the differential ultrasound intensity was calculated. Next, the ratio of the two greatest values of the autocorrelation was calculated, using a delay corresponding to the 10 Hz laser repetition rate. The value of this ratio was then converted to image intensity. The final image was created by pixel-wise multiplication of the two previously formed images. This map of BLInCs was then overlaid onto a B-mode image. A more detailed description of the formation of a background-free image can be found in the Supplementary Information. Contrast and contrast-to-noise ratio were calculated using previously reported methods (18).

Ultrasound Imaging of Lymph Node

All animal studies were performed under protocols approved by the Institutional Animal Care and Use Committee at The University of Texas at Austin.

A previously developed mouse model of lymph node drainage was used (30–32) in which a nude Nu/Nu mouse (Charles River Laboratories) was injected submucosally in the tongue with BLInCs. Prior to injection, the mouse was anesthetized with a combination of isoflurane (1.5%) and O_2 (2 L/min). A 30-gauge needle was used to inject 40 µL of as-prepared BLInCs over the course of approximately 10 s. The BLInCs were allowed to drain for 30 minutes at which point ultrasound imaging was performed on the cervical lymph nodes located in the mouse's neck. Clear ultrasound gel was used for acoustic coupling between the transducer to the mouse. Ultrasound images were acquired with a Vevo 2100 (VisualSonics) using a 40-MHz linear array transducer (MS-550) at a rate of 618 frames/second. Light with a wavelength of 1064 nm was generated by a Vibrant Nd:YAG laser (Opotek) operating at 10 Hz and coupled to a custom fiber bundle. The optical fluence of approximately 50 mJ/cm^2 irradiating the mouse was well below the safety limit of 100 mJ/cm^2 for human skin exposure established by the American National Standards Institute.(33) The ultrasound window was 4.08 mm wide, 15 mm deep with a 4 mm offset, and a focal depth of 9 mm. Immediately following the imaging, the mouse was euthanized *via* an overdose of isoflurane (5%) and cervical dislocation.

Results

Photographs of the dye dissolved in chloroform, a solution of blank droplets, and a solution of BLInCs indicate the presence of the dye in the droplet solution (Fig. 2a). The extinction spectrum of the dye exhibits peak absorption in the near-infrared range (Fig. 2b). A histogram of droplet diameters indicates their submicron size (Fig. 2c).

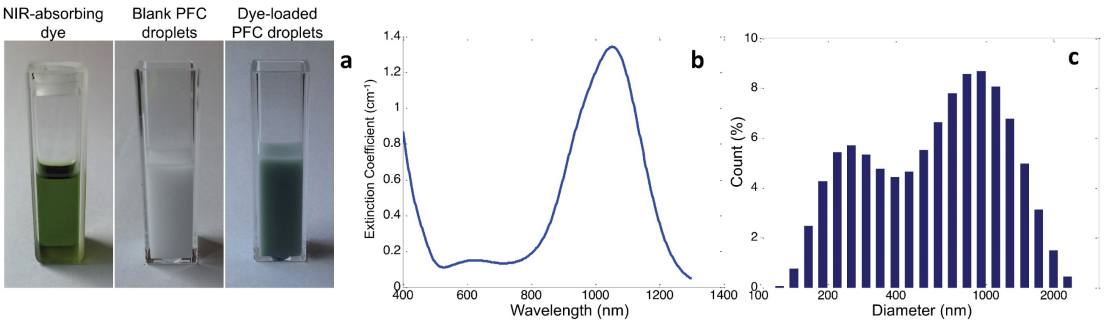

Figure 2. (a) Photographs of the (left) encapsulated dye, (middle) blank perfluorocarbon droplets, and (right) BLInCs. (b) Optical extinction spectrum of the encapsulated near-infrared absorbing dye. (c) Distribution of particle sizes.

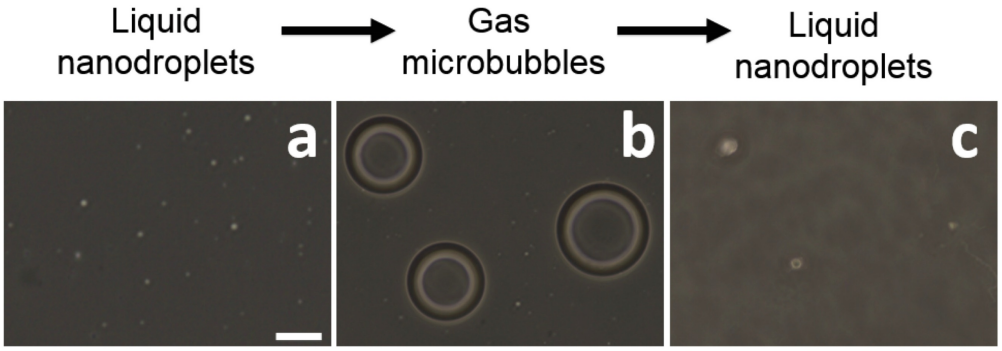

Figure 3. Light microscope images of BLInCs (a) before activation, (b) after activation, and (c) after recondensation into a liquid state. Scale bar = 20 μm.

Microscope images of the droplets before (Fig. 3a) and after (Fig. 3b) irradiation confirm an increase in particle diameter after vaporization, which is concurrent with other studies indicating a 5x increase in diameter.(15,34) Following recondensation, the droplets reverted to their original size (Fig. 3c).

The changes in echogenicity of a phantom (0.1% v/v BLInCs) exposed to various laser fluences demonstrate the importance of selecting proper laser energy. Perfluorohexane has a boiling point of 56° C, and the Laplace pressure of nano-sized droplets further stabilizes the BLInCs in a liquid state at physiological temperatures. When the BLInCs were irradiated below their vaporization threshold, they failed to exhibit any measurable changes in ultrasound echogenicity (Fig. 4a, black and Fig. 4b), and the background-free imaging technique was ineffective. When irradiated with sufficient energy, the BLInCs underwent rapid liquid-gas vaporization phase changes, followed immediately by gas-liquid condensation, resulting in brief increases in ultrasound signal from acoustic reflections by the bubbles (Fig. 4a, blue). However, identifying these momentary changes from the ultrasound images is difficult (Fig. 4c). When irradiated with much higher energy, the BLInCs underwent irreversible liquid-gas vaporization and exhibited a stable increase in ultrasound signal (Fig. 4a, red). While this provided lasting increase in echogenicity (Fig. 4d), a lack of 'blinking' behavior renders the image processing technique ineffective to suppress the background signal and provide a high contrast map of the BLInCs.

The two-part phase change of BLInCs was demonstrated using ultrasound imaging (650 frames/second) of a phantom with uniformly distributed BLInCs at a concentration of 0.001% v/v. The initially weakly scattering BLInCs (Fig. 5a) temporarily appear as bubbles (Fig. 5b) upon activation before recondensing back into their liquid state (Fig. 5c). While easy to see in a non-scattering phantom, the normal acoustic scattering of biological tissues disguises the phase change, especially at low BLInC concentrations.

Images of a phantom with a cylindrical inclusion show the contrast enhancement by the BLInCs in an environment that mimics the optical absorption and acoustic scattering of biological tissues.(35) The contrast of the BLInCs against an acoustic scattering background is not high using conventional ultrasound imaging techniques (contrast = 0.76, contrast-to-noise ratio = -0.73 dB) (Fig. 6a). However, a measurement of the ultrasound signal over time shows that pixels within the inclusion undergo reversible phase changes, while pixels in the background are unaffected by laser pulses (Fig. 6b). Difference images enhance the signal from the blinking particles while suppressing the constant background (Fig. 6c), because the derivative of an

unchanging signal is close to zero (Fig. 6d). While it was most common for the ultrasound signal to exhibit changes in the positive direction (BLInCs underwent a liquid-gas-liquid phase change), some pixels exhibited negative changes. This may have resulted from moving bubbles, or a reverse phase changed induced by positive pressure of the vaporized BLInCs nearby. For this reason, an absolute value of the derivative signal was used to capture a phase change in either direction. Further enhancement of the signal (Fig. 6e) was achieved using the autocorrelation of the derivative (Fig. 6f). This resulted in a large value at delay = 0 for pixels both inside and outside of the inclusion, but also yielded high values for delays at intervals equal to the pulse repetition frequency of the laser. By applying the image processing described in the Materials and Methods section, a high contrast map of the particles was constructed and overlaid onto an ultrasound background for anatomical reference. The image quality was greatly improved, and the location of the BLInCs was identified more easily (contrast = 2.8, contrast-to-noise ratio = 25 dB) (Fig. 6g).

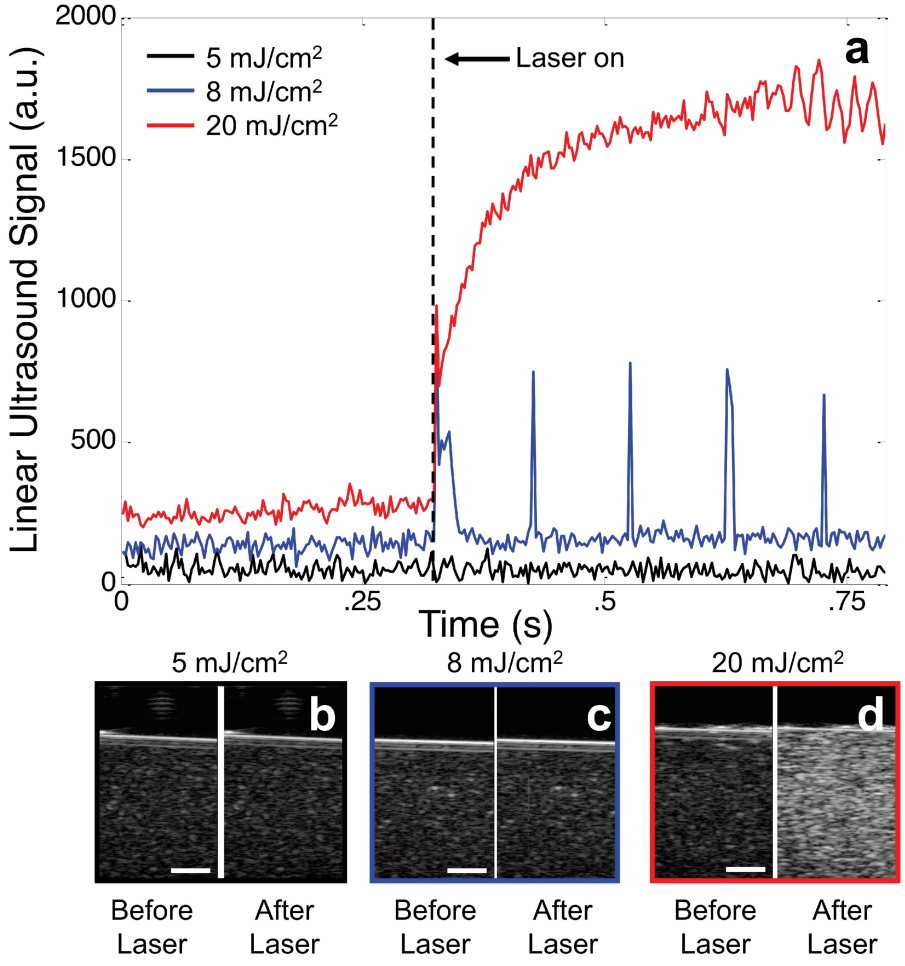

Figure 4. (a) Linear ultrasound signal from an image pixel of a phantom containing BLInCs irradiated with 5 mJ/cm² (black), 8 mJ/cm² (blue), and 20 mJ/cm² (red). Ultrasound images before and after irradiation at (b) 5, (c) 8, and (d) 20 mJ/cm². Scale bars = 1 mm.

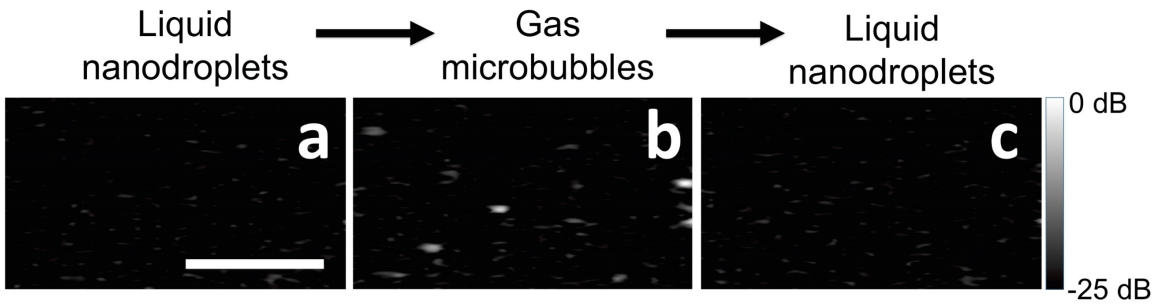

Figure 5. Ultrasound images of BLInCs (a) before activation, (b) after activation, and (c) after recondensation into a liquid state. Scale bar = 1 mm.

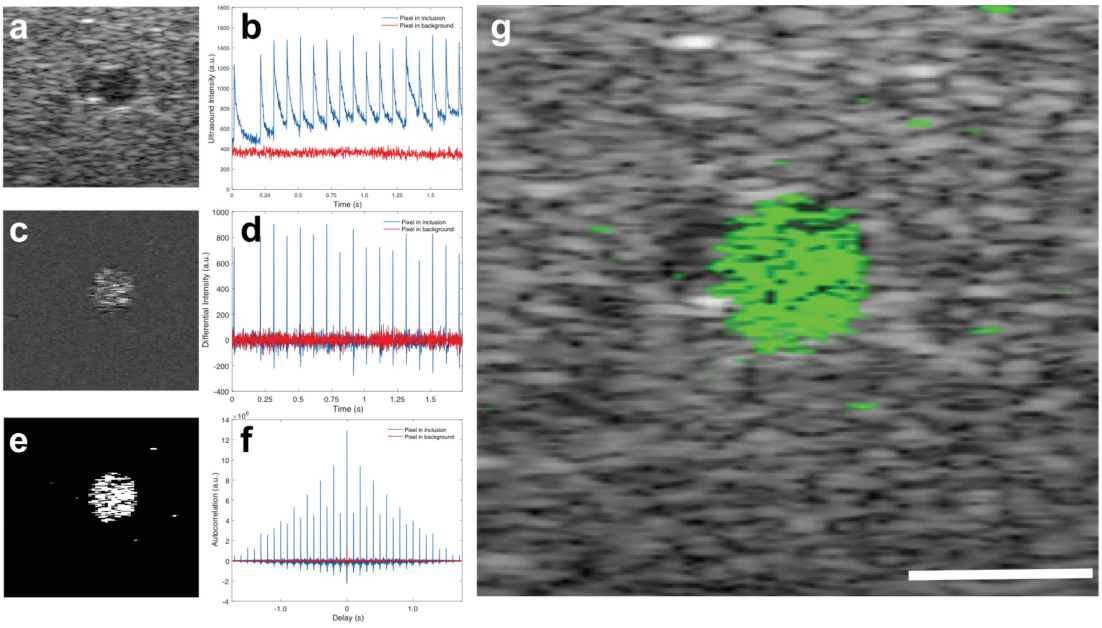

Figure 6. (a) Ultrasound image of a cross-section of a phantom with inclusion of BLInCs. (b) Linear ultrasound signal as a function of time for two pixels, one within the inclusion of BLInCs, and one in the background. (c) Image formed by subtracting an ultrasound image frame before particle activation from an image frame after particle activation. (d) Differential ultrasound signal as a function of time for the two featured pixels. (e) Image formed by processing to enhance the BLInCs and suppress the background. (f) Autocorrelation of the differential ultrasound signal for the two pixels. (g) Background-free map of the BLInCs (green) overlaid onto the ultrasound image of the phantom. Scale bar = 1 mm.

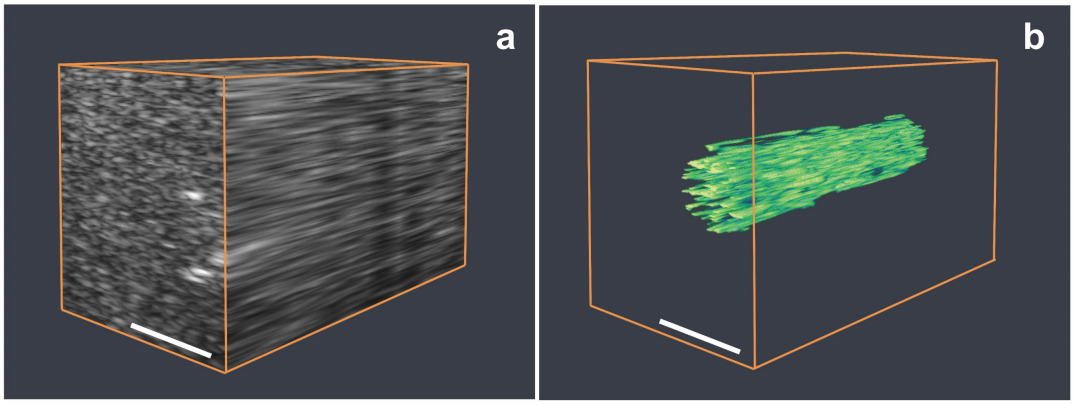

Figure 7. (a) Three-dimensional rendering of a series of B-mode ultrasound images of a phantom. (b) Three-dimensional rendering of the BLInCs signal after processing the ultrasound image data to distinguish BLInCs from the background. Scale bar = 2 mm.

A 3-dimensional map of the BLInCs was obtained by collecting and processing image data along several elevational planes. Figure 7a is an ultrasound 3D rendering of the phantom with the cylindrical inclusion of BLInCs. While some boundaries can be identified, the overall structure of the inclusion is difficult to discern. By applying the background-free imaging technique, the location of BLInCs was identified more clearly while suppressing the background signal of optical absorbers and acoustic scatterers (Fig. 7b). Identifying BLInCs in a biological environment with high sensitivity and contrast using could enable early detection of various disease markers.

In many types of cancer, identifying the sentinel lymph node (SLN) is critical for accurate staging, because it is the first lymph node to which metastasized cells drain from a tumor. A mouse model of lymphatic drainage demonstrates the utility of BLInCs in SLN mapping.(32) Although ultrasound imaging is routinely used for lymph node imaging, the SLN cannot be accurately identified from anatomy alone. Therefore, contrast agents are helpful in mapping the SLN. As in the phantom imaging, laser pulses were used to repeatedly activate the BLInCs. However, the changes in echogenicity were difficult to detect in real time (Fig. 8a-b) due to the low concentration of bubbles, the highly scattering background, the rapid recondensation of the BLInCs into their liquid state, and the dB scale of ultrasound images. The lymph node was roughly identified using anatomical reference from the conventional B-mode

images (Fig. 8b). Using the time-series data, the rapid, periodic changes in echogenicity distinguished the BLInCs from the background by processing the temporal characteristics of individual image pixels. This resulted in a background-free map of the BLInCs, which was overlaid onto an ultrasound image to visualize them in an anatomical reference (Fig. 8c). Here the BLInCs are seen throughout the volume of the lymph node, indicating rapid drainage via the lymphatic system, behavior that has been previously observed and reported for similarly sized particles.(36) Blinking signal was not observed in mice where there was no injection of BLInCs (Supplementary Fig. S6). The stability of perfluorohexane droplets *in vitro* (37) and perfluoropentane droplets *in vivo* (20) suggest that BLInCs can circulate through the vasculature for several hours. Prolonged imaging may be conducted due to the sensitivity of the imaging procedure and the ability of the BLInCs to undergo repeatable activation, which would allow sufficient time for their accumulation into extravascular tissues and/or attachment to molecular targets. Significant blinking signal appears at the surface of the skin. This is most likely due to bubbles at the skin/gel interface, which oscillate in the presence of photoacoustic signal generation following laser irradiation. This oscillation appears as blinking signal, so surface bubbles should be minimized during this imaging process.

Discussion

The BLInCs facilitate a new imaging technique for background-free images of injected particles. However, the activation laser energy must be appropriate to allow for transient droplet vaporization, accounting for optical absorption and scattering in biological tissues. The laser fluence required for vaporization in a non-scattering phantom (Fig. 4, 5) was lower than that in a phantom containing optical absorbers (Fig. 6, 7) or in a mouse lymph node (Fig. 8). Given the optical wavelength of activation and sensitivity of BLInCs to vaporization, it is feasible that they may be imaged at depths of > 2 cm. (38)

To achieve both particle stability over time as well as high contrast from their unique blinking behavior, it is important activate BLInCs with a laser fluence that achieves repeatable, reversible phase changes. This is most easily accomplished by imaging initially at low laser fluence, and then increasing the energy until the blinking behavior can be observed. Implementing a real-time imaging algorithm would aid in selecting appropriate laser fluence.

The irreversible vaporization of BLInCs (Fig. 4d) is possibly due to vaporization of larger BLInCs, coalescence of neighboring bubbles into larger stable bubbles, or diffusion of air into the cavity created by the bubble. Larger bubbles are less prone to recondense back into their liquid droplet form than very small bubbles.(27) However, smaller BLInCs require more laser energy to vaporize.(39–41) It is desirable to synthesize a monodisperse sample of droplets so that precise control over laser energy can maximize the vaporization efficiency and prevent irreversible vaporization. Stable bubble formation is ineffective for producing a background-free image, and the acoustic scattering from bubbles may mask any blinking behavior from smaller BLInCs.

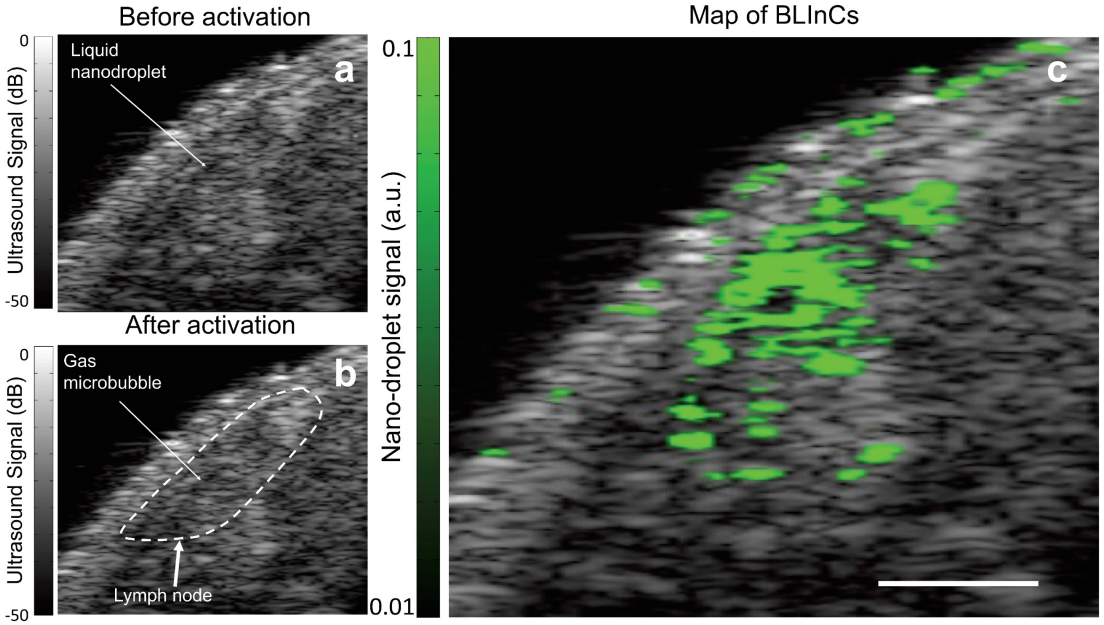

Figure 8. Ultrasound images of mouse tissue (a) before and (b) after optical irradiation, with a rough outline of the lymph node location. (c) The BLInCs signal, overlaid onto the ultrasound image, shows the location of the particles, which have accumulated in the node of the lymphatic system. Scale bar = 1 mm.

To construct a background-free image, the ultrasound image data was collected at a frame rate high enough to capture the rapid two-stage phase change of the BLInCs. The speed of the phase change (most notably recondensation) depends on several factors, including the size of the BLInCs and the likelihood of neighboring bubble coalescence following vaporization.(27) The likelihood of coalescence depends on the concentration of bubbles formed (either from a high concentration of BLInCs or from efficient vaporization by high laser fluence). Other factors may also affect speed of condensation, such as the stiffness of the surrounding medium and the ultrasound pressure field. It may be possible to characterize tissue properties by observing the dynamic behavior of the BLInCs in response to laser activation.

While more than ten laser pulses were used to form each of the images, this technique may be carried out using fewer laser pulses. If the autocorrelation or a similar approach is used to identify blinking pixels, at least two laser pulses are required, although greater image contrast will result when more phase changes are measured. The laser pulse repetition frequency determines the imaging frame rate, thus higher frame rate can be achieved by using lasers with much faster pulse repetition frequency.

Most pixel data of BLInCs exhibited an increase in echogenicity followed by a decrease in echogenicity at intervals corresponding to laser pulses. However, some pixels underwent a decrease in echogenicity followed by an increase, the opposite of what was expected. These data are possibly indicative of bubbles that moved while other BLInCs were being activated, or to surrounding pressure increases which induced bubble recondensation. To overcome this limitation, the absolute value of the difference image was used during formation of the background-free image.

Droplet vaporization has also been triggered with high intensity focused ultrasound (HIFU),(17,42) which could also be used to trigger BLInCs without a laser or optical absorber. However, due to the high boiling point of perfluorohexane, vaporization with HIFU may require intensity levels of up to 1,000 W/cm^2,(43) which is 500 times the safe recognized level for peripheral tissue,(44) compromising the safety of the imaging technique. Some research exists showing that the vaporization threshold of perfluorocarbon droplets can be reduced by incorporating nucleation seeds,(45,46) which may enable deeper, more sensitive activation of BLInCs.

The transient phase-change behavior of BLInCs makes them a valuable tool for high contrast biomedical imaging. Any injectable particles, however, must be made of materials approved for human use before clinical translation. While the BLInCs reported here encapsulate a near-infrared dye for improved optical penetration in tissue at 1064 nm,(47) similar particles have been made using clinically approved indocyanine green dye.(13) Thus it is feasible to synthesize BLInCs out of entirely approved materials to be used in a clinical setting.

BLInCs may be used as a therapeutic tool in addition to their high contrast imaging utility. Localized drug delivery could be achieved with these or similar triggerable nanodroplets, whereby drug is released upon activation of the particle and delivery to the site of interest is improved through nanodroplet extravasation, or intracellular droplet or drug uptake through sonoporation.(48,49) It is possible that the repeatable vaporization may provide sustained therapeutic benefit similar to the effects of microbubble-assisted HIFU therapy, which is unattainable through irreversible optical droplet vaporization alone. Additionally, imaging the BLInCs could identify the site of therapeutic payload.

Conclusion

The BLInCs introduced here facilitate a new technique for background-free imaging of nanoparticles using a conventional ultrasound imaging system. Due to their stability and small size, the droplets are capable of extended circulation time and extravasation, a key component of imaging on the molecular scale. The BLInCs are made to activate through a unique, laser-induced rapid sequence of two phase changes—vaporization and recondensation—which is processed into a background-free map of the particles. This imaging technique is highly sensitive to diluted particles. Due to their blinking behavior, individual BLInCs can be located among the vast acoustic scatterers present in tissue. These experiments identify BLInCs with high specificity and sensitivity in the optically absorbing and acoustically scattering background of a living mouse. Furthermore, cell-specific targeting has been achieved with similar perfluorocarbon microbubbles by conjugating various molecules to the particle shell.(50–53) The smaller size and enhanced circulation time of nanodroplets make them a feasible candidate for molecular imaging, expanding the performance of this nanoparticle-based ultrasound imaging platform.

Supplementary Material

Supplementary figures.
http://www.thno.org/v06p1866s1.pdf

Acknowledgements

The authors want to thank Kristina Hallam, Steven Yarmoska and Diego Dumani from the Georgia Institute of Technology for help conducting the phantom imaging experiment, collecting DLS particle size data, and performing laser fluence measurements, respectively. This work is supported by the National Institutes of Health under grants CA149740, EB008101 and CA158598, and by a grant from the Breast Cancer Research Foundation.

Competing Interests

The authors declare no competing financial interests.

References

1. Gramiak R, Shah Pm. Echocardiography of the aortic root. Invest Radiol. 1967 Dec;3(5):356–66.
2. Klibanov AL. Ligand-carrying gas-filled microbubbles: ultrasound contrast agents for targeted molecular imaging. Bioconjug Chem. 2005 Feb;16(1):9–17.
3. Chivers RC. The scattering of ultrasound by human tissues—Some theoretical models. Ultrasound Med Biol. 1977;3(1):1–13.
4. Senapati N, Lele PP, Woodin A. A Study of the Scattering of Sub-Millimeter Ultrasound from Tissues and Organs. In: 1972 Ultrasonics Symposium. 1972:59–63.
5. Stakutis VJ, Morse RW, Dill M, Beyer RT. Attenuation of Ultrasound in Aqueous Suspensions. J Acoust Soc Am. 1955 May 1;27(3):539–46.
6. Simpson DH, Chin CT, Burns PN. Pulse inversion Doppler: a new method for detecting nonlinear echoes from microbubble contrast agents. IEEE Trans Ultrason Ferroelectr Freq Control. 1999;46(2):372–82.
7. Miller DL. Ultrasonic detection of resonant cavitation bubbles in a flow tube by their second-harmonic emissions. Ultrasonics. 1981 Sep;19(5):217–24.
8. Needles A, Arditi M, Rognin NG, Mehi J, Coulthard T, Bilan-Tracey C, et al. Nonlinear Contrast Imaging with an Array-Based Micro-Ultrasound System. Ultrasound Med Biol. 2010 Dec;36(12):2097–106.
9. Bauer A, Hauff P, Lazenby J, Behren P von, Zomack M, Reinhardt M, et al. Wideband harmonic imaging: A novel contrast ultrasound imaging technique. Eur Radiol. 1999 Nov 1;9(3):S364–S367.
10. Goertz DE, Cherin E, Needles A, Karshafian R, Brown A, Burns PN, et al. High frequency nonlinear B-scan imaging of microbubble contrast agents. IEEE Trans Ultrason Ferroelectr Freq Control. 2005 Jan;52(1):65–79.
11. Prabhakar U, Maeda H, Jain RK, Sevick-Muraca EM, Zamboni W, Farokhzad OC, et al. Challenges and Key Considerations of the Enhanced Permeability and Retention Effect for Nanomedicine Drug Delivery in Oncology. Cancer Res. 2013 Apr 15;73(8):2412–7.
12. Ferrara K, Pollard R, Borden M. Ultrasound Microbubble Contrast Agents: Fundamentals and Application to Gene and Drug Delivery. Annu Rev Biomed Eng. 2007;9(1):415–47.
13. Hannah A, Luke G, Wilson K, Homan K, Emelianov S. Indocyanine Green-Loaded Photoacoustic Nanodroplets: Dual Contrast Nanoconstructs for Enhanced Photoacoustic and Ultrasound Imaging. ACS Nano. 2014 Jan 28;8(1):250–9.
14. Wilson K, Homan K, Emelianov S. Biomedical photoacoustics beyond thermal expansion using triggered nanodroplet vaporization for contrast-enhanced imaging. Nat Commun. 2012 Jan 10;3:618.
15. Strohm E, Rui M, Gorelikov I, Matsuura N, Kolios M. Vaporization of perfluorocarbon droplets using optical irradiation. Biomed Opt Express. 2011 May 4;2(6):1432–42.
16. Sheeran PS, Dayton PA. Phase-Change Contrast Agents for Imaging and Therapy. Curr Pharm Des. 2012 May 1;18(15):2152–65.
17. Rapoport N, Gao Z, Kennedy A. Multifunctional Nanoparticles for Combining Ultrasonic Tumor Imaging and Targeted Chemotherapy. J Natl Cancer Inst. 2007 Jul 18;99(14):1095–106.
18. Hannah AS, VanderLaan D, Chen Y-S, Emelianov SY. Photoacoustic and ultrasound imaging using dual contrast perfluorocarbon nanodroplets triggered by laser pulses at 1064 nm. Biomed Opt Express. 2014 Sep 1;5(9):3042.
19. Sheeran PS, Rojas JD, Puett C, Hjelmquist J, Arena CB, Dayton PA. Contrast-Enhanced Ultrasound Imaging and in Vivo Circulatory Kinetics with Low-Boiling-Point Nanoscale Phase-Change Perfluorocarbon Agents. Ultrasound Med Biol. 2015 Mar;41(3):814–31.
20. Rapoport N, Nam K-H, Gupta R, Gao Z, Mohan P, Payne A, et al. Ultrasound-mediated tumor imaging and nanotherapy using drug loaded, block copolymer stabilized perfluorocarbon nanoemulsions. J Controlled Release. 2011 Jul 15;153(1):4–15.
21. Akers WJ, Kim C, Berezin M, Guo K, Fuhrhop R, Lanza GM, et al. Noninvasive Photoacoustic and Fluorescence Sentinel Lymph Node Identification using Dye-Loaded Perfluorocarbon Nanoparticles. ACS Nano. 2011 Jan 25;5(1):173–82.
22. Larson-Smith K, Pozzo DC. Pickering Emulsions Stabilized by Nanoparticle Surfactants. Langmuir. 2012 Aug 14;28(32):11725–32.
23. Asami R, Kawabata K. Repeatable vaporization of optically vaporizable perfluorocarbon droplets for photoacoustic contrast enhanced imaging. In: Ultrasonics Symposium (IUS), 2012 IEEE International. 2012:1200–3.
24. Arnal B, Perez C, Wei C-W, Xia J, Lombardo M, Pelivanov I, et al. Sono-photoacoustic imaging of gold nanoemulsions: Part I. Exposure thresholds. Photoacoustics. 2015 Mar;3(1):3–10.
25. Arnal B, Wei C-W, Perez C, Nguyen T-M, Lombardo M, Pelivanov I, et al. Sono-photoacoustic imaging of gold nanoemulsions: Part II. Real time imaging. Photoacoustics. 2015 Mar;3(1):11–9.
26. Reznik N, Williams R, Burns PN. Investigation of Vaporized Submicron Perfluorocarbon Droplets as an Ultrasound Contrast Agent. Ultrasound Med Biol. 2011 Aug;37(8):1271–9.
27. Reznik N, Shpak O, Gelderblom EC, Williams R, de Jong N, Versluis M, et al. The efficiency and stability of bubble formation by acoustic vaporization of submicron perfluorocarbon droplets. Ultrasonics. 2013 Sep;53(7):1368–76.
28. Jacques SL. Optical properties of biological tissues: a review. Phys Med Biol. 2013;58(11):R37.
29. Hernandez Y, Nicolosi V, Lotya M, Blighe FM, Sun Z, De S, et al. High-yield production of graphene by liquid-phase exfoliation of graphite. Nat Nanotechnol. 2008 Sep;3(9):563–8.
30. Luke GP, Emelianov SY. Optimization of in vivo spectroscopic photoacoustic imaging by smart optical wavelength selection. Opt Lett. 2014 Apr 1;39(7):2214–7.
31. Luke GP, Myers JN, Emelianov SY, Sokolov KV. Sentinel lymph node biopsy revisited: ultrasound-guided photoacoustic detection of micrometastases using molecularly targeted plasmonic nanosensors. Cancer Res. 2014 Aug 8;canres.0796.2014.
32. Myers JN, Holsinger FC, Jasser SA, Bekele BN, Fidler IJ. An Orthotopic Nude Mouse Model of Oral Tongue Squamous Cell Carcinoma. Clin Cancer Res. 2002 Jan 1;8(1):293–8.
33. American National Standards Institute Inc. American National Standard for Safe Use of Lasers. Laser Institute of America (Laser Institute of America, Orlando, FL); 2007.
34. Reznik N, Williams R, Burns PN. Optical and acoustic characterization of vapourized perfluorocarbon droplets as ultrasound contrast agents. In: Ultrasonics Symposium (IUS), 2009 IEEE International. 2009: 2778–81.
35. Cook JR, Bouchard RR, Emelianov SY. Tissue-mimicking phantoms for photoacoustic and ultrasonic imaging. Biomed Opt Express. 2011 Nov 1;2(11):3193.
36. Luke GP, Bashyam A, Homan KA, Makhija S, Chen Y-S, Emelianov SY. Silica-coated gold nanoplates as stable photoacoustic contrast agents for sentinel lymph node imaging. Nanotechnology. 2013 Nov 15;24(45):455101.
37. Simons JMM, Kornmann LM, Reesink KD, Hoeks APG, Kemmere MF, Meuldijk J, et al. Monodisperse perfluorohexane emulsions for targeted ultrasound contrast imaging. J Mater Chem. 2010;20(19):3918.
38. Esenaliev RO, Karabutov AA, Oraevsky AA. Sensitivity of laser opto-acoustic imaging in detection of small deeply embedded tumors. IEEE J Sel Top Quantum Electron. 1999 Jul;5(4):981–8.
39. Fabiilli ML, Haworth KJ, Fakhri NH, Kripfgans OD, Carson PL, Fowlkes JB. The role of inertial cavitation in acoustic droplet vaporization. IEEE Trans Ultrason Ferroelectr Freq Control. 2009 May;56(5):1006–17.
40. Kripfgans OD, Fabiilli ML, Carson PL, Fowlkes JB. On the acoustic vaporization of micrometer-sized droplets. J Acoust Soc Am. 2004 Jul 1;116(1):272–81.
41. Schad KC, Hynynen K. In vitro characterization of perfluorocarbon droplets for focused ultrasound therapy. Phys Med Biol. 2010;55(17):4933.
42. Miller DL, Kripfgans OD, Fowlkes JB, Carson PL. Cavitation nucleation agents for nonthermal ultrasound therapy. J Acoust Soc Am. 2000 Jun 1;107(6):3480–6.
43. Asami R, Azuma T, Kawabata K. Fluorocarbon droplets as next generation contrast agents - their behavior under 1 #x2013;3 MHz ultrasound. In: Ultrasonics Symposium (IUS), 2009 IEEE International. 2009: 1294–7.
44. Singh PDVR. Safety Standards for Medical Ultrasound Systems. In: Magjarevic R, Nagel JH, editors. World Congress on Medical Physics and Biomedical Engineering 2006 [Internet]. Springer Berlin Heidelberg; 2007: 2764–6. (IFMBE Proceedings). Available from: http://link.springer.com/chapter/10.1007/978-3-540-36841-0_697
45. Lee JY, Carugo D, Crake C, Owen J, de Saint Victor M, Seth A, et al. Nanoparticle-Loaded Protein–Polymer Nanodroplets for Improved Stability and Conversion Efficiency in Ultrasound Imaging and Drug Delivery. Adv Mater. 2015 Oct 1;27(37):5484–92.
46. Matsuura N, Williams R, Gorelikov I, Chaudhuri J, Rowlands J, Hynynen K, et al. Nanoparticle-loaded perfluorocarbon droplets for imaging and therapy. In: Ultrasonics Symposium (IUS), 2009 IEEE International. 2009: 5–8.
47. Homan K, Kim S, Chen Y-S, Wang B, Mallidi S, Emelianov S. Prospects of molecular photoacoustic imaging at 1064 nm wavelength. Opt Lett. 2010 Aug 1;35(15):2663.
48. Rapoport N. Phase-shift, stimuli-responsive perfluorocarbon nanodroplets for drug delivery to cancer. Wiley Interdiscip Rev Nanomed Nanobiotechnol. 2012 Sep 1;4(5):492–510.

49. Gao Z, Kennedy AM, Christensen DA, Rapoport NY. Drug-loaded nano/microbubbles for combining ultrasonography and targeted chemotherapy. Ultrasonics. 2008 Aug;48(4):260–70.
50. Villanueva FS, Jankowski RJ, Klibanov S, Pina ML, Alber SM, Watkins SC, et al. Microbubbles Targeted to Intercellular Adhesion Molecule-1 Bind to Activated Coronary Artery Endothelial Cells. Circulation. 1998 Jul 7;98(1):1–5.
51. Lindner JR, Song J, Christiansen J, Klibanov AL, Xu F, Ley K. Ultrasound Assessment of Inflammation and Renal Tissue Injury With Microbubbles Targeted to P-Selectin. Circulation. 2001 Oct 23;104(17):2107–12.
52. Ellegala DB, Leong-Poi H, Carpenter JE, Klibanov AL, Kaul S, Shaffrey ME, et al. Imaging Tumor Angiogenesis With Contrast Ultrasound and Microbubbles Targeted to αvβ3. Circulation. 2003 Jul 22;108(3):336–41.
53. Willmann JK, Paulmurugan R, Chen K, Gheysens O, Rodriguez-Porcel M, Lutz AM, et al. US Imaging of Tumor Angiogenesis with Microbubbles Targeted to Vascular Endothelial Growth Factor Receptor Type 2 in Mice. Radiology. 2008 Feb 1;246(2):508–18.